

# Original Research

## Antibody-based delivery of interleukin-9 to neovascular structures: Therapeutic evaluation in cancer and arthritis

Baptiste Gouyou<sup>1</sup>, Tiziano Ongaro<sup>1</sup>, Samuele Cazzamalli<sup>1</sup>, Roberto De Luca<sup>1</sup>, Anne Kerschenmeyer<sup>1</sup>, Philippe Valet<sup>2</sup>, Alessandra Villa<sup>1</sup>, Dario Neri<sup>3</sup> and Mattia Matasci<sup>1</sup> 

<sup>1</sup>Philochem AG, Libernstrasse 3, Otelfingen 8112, Switzerland; <sup>2</sup>Institut des Maladies Métaboliques et Cardiovasculaires, INSERM U1048, Université de Toulouse, UPS, Cedex 4, Toulouse 31432, France; <sup>3</sup>Department of Chemistry and Applied Biosciences, Swiss Federal Institute of Technology, Zurich 8093, Switzerland

Corresponding author: Mattia Matasci. Email: mattia.matasci@philogen.com

### Impact statement

Although treatments in oncology and arthritis have made great progress in recent years, there is a constant need to develop new and more effective therapies for these pathologies. IL9 has been suggested to play an important role in antitumor immunity in certain cancer types, and to induce the resolution of chronic inflammation in arthritis. In the present study, we have developed a new IL9-based immunocytokine with improved *in vivo* targeting efficacy and tested its therapeutic efficacy in preclinical models of cancer and rheumatoid arthritis. Our findings, which are partially in contrast with the previously reported therapeutic activity of IL9, may be significant for a further understanding of the role played by this cytokine in cancer and inflammatory diseases.

### Abstract

Interleukin-9 is a cytokine with multiple functions, including the ability to activate group 2 innate lymphoid cells, which has been postulated to be therapeutically active in mouse models of arthritis. Similarly, interleukin-9 has been suggested to play an important role in tumor immunity. Here, we describe the cloning, expression, and characterization of three fusion proteins based on murine interleukin-9 and the F8 antibody, specific to the alternatively spliced EDA domain of fibronectin. EDA is strongly expressed in cancer and in various arthritic conditions, while being undetectable in the majority of healthy organs. Interleukin-9-based fusion proteins with an irrelevant antibody specific to hen egg lysozyme served as negative control in our study. The fusion proteins were characterized by quantitative biodistribution analysis in tumor-bearing mice using radioiodinated protein preparations. The highest tumor uptake and best tumor:organ ratios were observed for a format, in which the interleukin-9 moiety was flanked by two units of the F8 antibody in single-chain Fv format. Biological activity of interleukin-9 was retained when the payload was fused to antibodies. However, the targeted delivery of interleukin-9 to the disease site resulted in a modest anti-

tumor activity in three different murine models of cancer (K1735M2, CT26, and F9), while no therapeutic benefit was observed in a collagen induced model of arthritis. Collectively, these results confirm the possibility to deliver interleukin-9 to the site of disease but cast doubts about the alleged therapeutic activity of this cytokine in cancer and arthritis, which has been postulated in previous publications.

**Keywords:** Tumor targeting, rheumatoid arthritis targeting, fibronectin, immunocytokines, interleukin-9, armed-antibody

**Experimental Biology and Medicine 2021; 246: 940–951. DOI: 10.1177/1535370220981578**

### Introduction

Interleukin-9 (IL9) is a multifunctional cytokine that has been originally identified as a T-cell and mast cells growth factor.<sup>1</sup> IL9 is secreted by mast cells and CD4<sup>+</sup> T cells, including Th2, Th9, Th17, Treg, and NK cells<sup>2</sup> following stimulation by TGF $\beta$  and IL4.<sup>3</sup> Its biological action is mediated by the heterodimeric receptor IL9-R comprising a specific IL9 receptor  $\alpha$ -chain and the common  $\gamma$ -chain cytokine receptor.<sup>4</sup> IL9 has been demonstrated to play an important role in a variety of physiological and pathological conditions including pathogen immunity,<sup>5,6</sup> allergic

inflammation,<sup>7,8</sup> and the immune regulation of cancer progression.<sup>9,10</sup>

The role of IL9 in tumor growth is controversial, whereas IL9 has been correlated to the progression of hematological malignancies both in mouse<sup>11</sup> and human,<sup>12</sup> more recently IL9 dependent anti-cancer activity have been reported in a variety of solid tumor models including melanomas<sup>13</sup> and colon carcinomas.<sup>14,15</sup>

According to its postulated immunomodulatory activity, IL9-based therapies have been investigated in preclinical models of cancer and inflammation. In particular, Purwar

and collaborators investigated the tumor immunity provided by IL9 in a preclinical therapeutic setting.<sup>13</sup> In the B16F10 melanoma models, they demonstrated the ability of recombinant IL9 to impair tumor cell growth by a mechanism dependent on mast cells but not on T or B cells. The authors obtained similar results when recombinant IL9 was administered to mice bearing Lewis Lung carcinoma tumors suggesting a potential use of IL9-based therapies for the treatment of diverse cancer types.

More recently, Rauber and collaborators have identified IL9 as a key player in the resolution of rheumatoid arthritis in murine models of antigen-induced arthritis (AIA) and serum-induced arthritis (SIA).<sup>16</sup> In their proposed mode of action, IL9 would promote ILC2 proliferation through an autocrine loop, finally resulting in the activation of Treg cells via a GITR/GITRL and ICOS/ICOSL dependent mechanism. The authors used a gene therapy approach based on hydrodynamic gene delivery to mediate recombinant expression of an IL9 cDNA construct in the treated mice. The *in vivo* levels of recombinant IL9 in arthritic mice were not measured, but a strong inhibition of disease progression, reduced tissue damage, and bone loss was reported compared to control mice treated with a mock construct. Collectively, the published work on the therapeutic use of IL9 prompted us to develop and evaluate new IL9-based immunocytokines and test them in preclinical models of cancer and arthritic diseases.

Various cytokine-based therapeutics may benefit from a targeted delivery to the site of disease, helping spare normal organs.<sup>17-19</sup> We have previously described an antibody-IL9 fusion protein and reported an unexpected impact of protein glycoform variation on tumor targeting performance.<sup>20</sup> Specifically, we used the F8 antibody, which recognizes the alternatively spliced EDA domain of fibronectin, a marker of tumor angiogenesis and of tissue remodeling.<sup>21</sup> F8 reacts with murine and human EDA with identical affinity, since the target antigen features only three amino acid substitutions from mouse to man.<sup>21</sup> EDA is strongly expressed in the majority of solid tumors,<sup>22,23</sup> lymphomas,<sup>24</sup> and in the bone marrow and chloroma lesions of acute leukemias<sup>25</sup> with a characteristic perivascular staining pattern, while the antigen is virtually undetectable in normal adult organs, exception made for the female reproductive system.<sup>26</sup>

The tumor-targeting ability of the F8 antibody and of its derivatives has been established using radiolabeled protein preparations and quantitative biodistribution analysis.<sup>20,21,27-30</sup> Interestingly, pathological specimens from diseased tissues undergoing substantial remodeling (e.g. endometriosis, arthritis, psoriasis, atherosclerosis, vasculopathy and certain inflammatory bowel conditions) have been shown to be strongly positive for EDA(+)-fibronectin. The ability of F8 derivatives to preferentially localize at sites of chronic inflammation has been shown in mouse models<sup>26,27,31-34</sup> and in patients with rheumatoid arthritis.<sup>35</sup>

In this article, we describe the design, expression, and characterization of three recombinant formats of IL9-based fusion proteins based on the EDA-targeting F8 antibody. IL9-fusions with the KSF antibody, specific for hen egg lysozyme, served as negative control with irrelevant

specificity in the mouse. The fusion proteins were characterized in terms of their biochemical parameters, IL9 activity, and tumor-targeting performance in biodistribution analysis after radioiodination. One of the formats, featuring the IL9 moiety flanked by two units of the F8 antibody in single-chain Fv (scFv) format, exhibited the best tumor targeting performance, with tumor:blood ratios >10:1, 24 h after intravenous administration. Whereas, a low increase of immune cells infiltration within tumors was observed, IL9 fusion proteins displayed only minimal therapeutic activity in three immunocompetent mouse models of cancer (K1735M2, CT26, and F9) at the maximal tolerated dose. Similarly, no retardation of disease progression was observed in the collagen-induced model of arthritis in mice. These results confirm that IL9 can be efficiently delivered to sites of disease with high expression of EDA *in vivo*, but cast doubts about the alleged translational therapeutic relevance of IL9 for the treatment of cancer and of chronic inflammatory conditions.

## Materials and methods

### Cloning of IL9-based fusion proteins

The genes encoding the antibody fusion proteins used in this study were generated by the assembly of multiple PCR fragments using as starting templates cDNA encoding for the anti EDA F8 antibody<sup>20,21,27-30</sup> or the irrelevant anti hen-lysozyme KSF antibody,<sup>35</sup> either in scFv or diabody formats, and the murine IL9 (AA 19-144). The assembled constructs were inserted into the HindIII/NotI sites of the pcDNA3.1 (Invitrogen) mammalian expression vector. Primers used for the amplification and assembly of the different constructs are listed in the Supplementary Table 1.

The pcDNA3.1-F8IL9F8 vector contains the murine IL9 sequence flanked at both the N- and C- termini by a 10-mer peptidic linker and the F8 antibody in scFv format. A leader sequence from murine IgG was used for protein secretion. The pcDNA3.1-KSFIL9KSF contains a similar insert where the two F8 moieties were replaced by two copies of the KSF antibody in scFv format. The pcDNA3.1-F8IL9 and pcDNA3.1-IL9F8 carry an insert consisting of the F8 antibody in diabody format fused either to the N- (pcDNA3.1-F8IL9) or C- (pcDNA3.1-IL9F8) terminus of IL9 via a 15-mer amino acidic linker. As well in these two vectors, a murine IgG leader sequence was used for protein secretion.

### Protein expression, purification, and characterization

The IL9-based fusion proteins (F8IL9F8, KSFIL9KSF, F8IL9, and IL9F8) were expressed by transient gene expression in CHO cells.<sup>36</sup> For transfection,  $4 \times 10^6$  cells/mL cells were resuspended in ProCHO-4 Medium (Lonza) supplemented with 4 mM Ultraglutamine (Lonza); 0.625  $\mu$ g of plasmid DNAs per million cells followed by 2.5  $\mu$ g polyethyleneimine per million cells (Polysciences) were added to the cells and gently mixed. Transfected cultures were incubated in a shaking incubator at 31°C with 5% CO<sub>2</sub> atmosphere shaking at 120 r/min for six days. The fusion proteins were purified by affinity chromatography using protein A affinity chromatography (Sino biological) according to the protocol

provided by the supplier. Following elution, proteins were finally dialyzed against PBS. Purified proteins were characterized for their size and homogeneity by SDS-PAGE and size exclusion chromatography, respectively. For SDS-PAGE analysis, proteins were run under reducing and non-reducing conditions on 10 or 12% acrylamide gels (Invitrogen) and stained using Coomassie blue. Size-exclusion chromatography was performed on an ÄKTA FPLC system using a Superdex 200 increase 10/300GL column (GE Healthcare). Protein binding affinity was performed by surface plasmon resonance using a BIAcore X100 instrument using a CM5 chip coated with recombinant fibronectin 11A12 domain. Samples were injected as serial-dilution, using a concentration range from 1 mM to 125 nM. The melting temperature of the different fusion proteins was determined using a StepOne real-Time PCR system (Applied Biosystems) in combination with the Protein Thermal Shift™ kit (Applied Biosystems).

### Immunofluorescence analysis of EDA expression

For biotinylation, 250 µg of fusion proteins were mixed to 50 µg of Biotin-NHS (Invitrogen) in a total volume of 1 mL. Reactions were gently agitated at room temperature for 1 h prior to removal of unreacted Biotin-NHS by size exclusion chromatography using PD-10 columns (GE Healthcare). Elution was performed using PBS. Immunofluorescence staining was performed on three different frozen tissues: F9 teratocarcinoma tumors from 129/Sv mice, and healthy human basal and chorionic placenta. Frozen sections (8 µm) were fixed by ice-cold acetone and blocked with 20% fetal bovine serum in PBS. Detection of EDA-positive fibronectin was performed using biotinylated fusion proteins followed by Streptavidin Alexa 488 (Invitrogen). In parallel, the neo-vasculature marker CD31 was detected using either rat anti-mouse CD31 (BD Pharmingen) or mouse anti-human CD31 (eBiosciences) followed by Donkey Anti Rat-IgG-Alexa Fluor™ 594 (Invitrogen), or Goat Anti Mouse-IgG-Alexa Fluor™ 594 (Invitrogen), respectively.

### In vitro bioactivity assay

The bioactivity of mIL9-based fusion proteins was tested by a proliferation assay using MC/9 cells (ATCC). These mast cells derived from mouse liver were expanded in suspension in DMEM, supplemented with 10% FBS, 10% rat T-Stim, 2 mM UltraGlutamine, and 0.05 mM  $\beta$ -MercaptoEtOH. MC/9 cells were seeded at 40,000 cells per well in 96 wells plates in 200 µL of culturing medium (with 5% FBS and 2.5% rat T-Stim). Murine IL9-based fusion proteins and commercial murine IL9 (Peprotech) were added to the cells in serial dilution (from 28 nM until 0.1 pM). After 70 h of incubation at 37°C with 5% CO<sub>2</sub> atmosphere, 20 µL of Cell Titer Aqueous One Solution (Promega) was added to the wells and after incubation of 2 h at 37°C the absorption at 492 nm was measured.

### Radiolabeled biodistribution and tumor therapies

*In vivo* experiments on tumor models were performed in agreement with the Swiss regulations and under a project license granted by the cantonal veterinary office (ZH027/15 for biodistribution and ZH004/18 for therapies). F9 teratocarcinoma cells (ATCC) were grown in DMEM (Life Technologies) supplemented with 10% FBS using 0.1% gelatin-coated tissue culture flasks; 129/Sv mice (8 weeks old, Charles River) were injected on the right flank with  $13 \times 10^6$  F9 teratocarcinomas. To assess tumor targeting in the F9 model, mice were grouped ( $n = 3$ ) when all tumors reached at least 200 mm<sup>3</sup>. *In vivo* targeting was evaluated by biodistribution analysis as described previously<sup>37</sup>; 100 µg of each fusion protein were radioiodinated with <sup>125</sup>I and Chloramine T hydrate and purified on a PD10 column (GE Healthcare), as described previously.<sup>37</sup> Approximately 10 µg of radiolabeled proteins were injected into the lateral tail vein. Mice were sacrificed 24 h after injection. Organs were weighed and radioactivity was counted using a Packard Cobra gamma counter (Packard, Meriden, CT, USA). Values are given as percentage of the injected dose per gram of tissue (%ID/g  $\pm$  standard error). K1735M2 melanomas were grown in DMEM (Life Technologies) supplemented with 10% FBS. C3H mice (eight weeks old, Janvier) were injected on the right flank with  $5 \times 10^6$  cells. Treatment started as soon as an average tumor size of >100 mm<sup>3</sup> was reached, mice were randomized and grouped ( $n = 5$  for IL9-based proteins,  $n = 4$  for PBS). Mice were injected three times every second day with the test article intravenously (i.v.) in the lateral tail vein; 200 µg of F8IL9F8 or KSFIL9KSF were injected, while PBS was injected at similar volume. CT26 colon carcinoma cells (ATCC) were grown in DMEM (Life Technologies) supplemented with 10% FBS. Balb/c mice (eight weeks old, Janvier) were injected on the right flank with  $15 \times 10^6$  cells. For therapies experiments with the CT26 cells, treatment started as soon as an average tumor size of >120 mm<sup>3</sup> was reached, mice were randomized and grouped ( $n = 5$ ). Either 200 µg or 100 µg of F8IL9F8 or equivalent volume of PBS were injected i.v. with the same schedule as the K1735M2 therapy. For F9 teratocarcinoma bearing mice, treatment started as soon as an average tumor size of >70 mm<sup>3</sup> was reached, mice were randomized and grouped ( $n = 5$ ); 200 µg F8IL9F8 or KSFIL9KSF were injected and the same volume of PBS was injected for the control group. Mice were injected i.v. with the same schedule as the K1735M2 therapy. For the three models, tumor volume was measured every day and the experiments were performed in a blind fashion. The therapy was discontinued by animal sacrifice when the weight loss exceeded  $-15\%$  or tumor volumes were exceeding 1500 mm<sup>3</sup>. Data are expressed as the mean volume  $\pm$  SEM. Differences between therapy groups were analyzed by two-way ANOVA multiple comparisons (Bonferroni corrected) using GraphPAD Prism (GraphPad Software, Inc.).

### Immunofluorescence analysis for ex vivo targeting and immune cells infiltrates studies

For FITC labeling, 1 mg of fusion protein was dialyzed in 0.1 M NaCO<sub>3</sub> pH 9 then mixed with 25 µg of FITC (ACROS

organics) in a total volume of 0.5 mL. Reactions were gently agitated at 4°C overnight prior to removal of unreacted FITC by size exclusion chromatography using PD-10 columns (GE Healthcare). Elution was performed using PBS. The *ex vivo* detection of the test articles was performed 24 h after i.v. injection of 160 µg of the FITC-labeled proteins (F8IL9F8 and KSFIL9KSF) or PBS as control. Mice were sacrificed and tumors were OCT embedded. Frozen sections (8 µm) were fixed by ice-cold acetone and blocked with 20% fetal bovine serum in PBS. Detection of the test articles was performed using a rabbit anti-FITC IgG (Biorad) followed by anti-rabbit IgG Alexa Fluor™ 488 (Invitrogen). The neovasculature marker CD31 was detected using a rat anti-mouse CD31 (BD Pharmingen) followed by Donkey Anti Rat-IgG-Alexa Fluor™ 594 (Invitrogen). Sections were counter-stained with DAPI.

For the analysis of immune infiltrate into the tumors, mice received F8IL9F8 ( $n=2$ ), KSFIL9KSF ( $n=1$ ) or PBS ( $n=1$ ) according to the same setting used in the therapy experiments (e.g. dose, schedule, tumor volume); 24 h after the last injection, K1735M2 and CT26 bearing mice were sacrificed and tumor was OCT embedded. Frozen sections (8 µm) were fixed by ice-cold acetone and blocked with 20% fetal bovine serum in PBS. Detection of the immune cells infiltrates was performed using rat anti-mCD8 (Biolegend), rat anti-mCD4 (Biolegend), rat anti-mFoxP3 (Invitrogen), or rat anti-mCD335 (NKp46) (Biolegend). Goat anti-rat IgG Alexa Fluor™ 488 (Invitrogen) was used as detection antibody. Slides were counter stained with DAPI prior analysis. Sections were analyzed using an Axioskop2 mot plus microscope (Zeiss); pictures have been acquired with 10× magnification. For quantification of immune cells infiltrates, six fields of each section were analyzed, and the percentage of stained area was calculated by ImageJ.

### Rheumatoid arthritis therapy

For the collagen-induced arthritis (CIA) experiments in mice, DBA/1J males (8–10 weeks old, Taconic Biosciences) were immunized by subcutaneous (s.c.) injection in the tail of an emulsion of bovine type II collagen in Completes Freund's Adjuvant (CFA) (Hooke Laboratories). Eighteen days later, a booster injection of bovine collagen/IFA (Hooke Laboratories) was given to the mice by s.c. injection in the tail. Mice were scored every other day, the final CIA score represents the scoring sum of all 4 paws (0 = normal; 1 = one toe inflamed and swollen; 2 = more than one toe, but not entire paw inflamed and swollen or mild inflammation and swelling of entire paw; 3 = entire paw inflamed and swollen; and 4 = very inflamed and swollen paw). CIA scoring was performed blind. At the onset of the disease, animals were randomized before receiving their first injection; 150 µg or 50 µg ( $n=15$ ) of F8IL9F8 ( $n=15$ ) or PBS ( $n=15$ ) were injected in a final volume of 150 µL three times every second day i.v. in the lateral tail vein. Dexamethasone was daily injected intraperitoneally (i.p.) at 0.5 mg/kg.

## Results

### All IL9 fusion proteins exhibit a good manufacturability profile

Different IL9-based fusion proteins were successfully expressed by transient gene expression (TGE) in Chinese hamster ovary (CHO) cells (Figure 1). The purified fusion proteins exhibited favorable biochemical properties as confirmed by SDS-PAGE and size exclusion chromatography (Figure 1(a) to (c)). EDA-binding kinetic was analyzed by surface plasmon resonance (SPR). SPR analysis showed comparable nanomolar range apparent KD for all fusion proteins: 3.4 nM, 5.2 nM, and 2.9 nM for F8IL9, IL9F8, and F8IL9F8, respectively (Figure 1(a) to (c)). The bioactivity of the murine IL9-based fusion proteins has been assessed by their ability to stimulate the proliferation of MC/9 cells. In this assay, the three IL9-based fusion proteins showed similar activity with EC50 values of 38 pM (F8IL9F8), 21 pM (IL9F8), and 40 pM (F8IL9). The fusion of IL9 to the F8 antibody may slightly impair its function as a commercial mIL9 preparation showed a 10-fold higher biological activity (EC50 = 4 pM). The comparative analysis of N- or C-terminal IL9 fusions showed that the arrangement of the different moieties did not affect its biological activity (Figure 1(d)). The single chain Fv-based variant of the fusion protein (F8IL9F8) displayed a 3°C increased melting temperature compared to the two variants based on the diabody format (Figure 1(e)), suggesting a better thermal stability. Indeed, when the F8IL9F8 variant was stored for up to seven days at 4°C or 37°C or when tested over three cycles of freeze and thawing, no sign of aggregation, degradation, or protein loss could be detected by size exclusion chromatography or SDS-PAGE analysis (data not shown). Taken together, these experiments suggest an overall better stability of the F8IL9F8 fusion protein.

### The format F8IL9F8 shows better *in vivo* targeting abilities

In order to test whether the IL9 fusion proteins retain the ability to bind EDA+ fibronectin on newly formed vascular structures, we performed immunofluorescence experiments on EDA-positive tissue sections (i.e. human placenta and F9 tumors).<sup>21</sup> The three fusion proteins selectively bound to neovasculature structures in both murine F9 teratocarcinoma and human placenta sections as confirmed by the co-localization with an anti-CD31 neovascular marker (Figure 2(e) and (f)). Subsequently, the *in vivo* targeting performance of the three IL9 fusion proteins was tested by biodistribution analysis in tumor bearing mice. Purified fusion proteins were radiolabeled with Iodine 125 and 10 µg of each variant was injected into immunocompetent mice bearing F9 murine teratocarcinoma. The three variants were able to selectively localize to the tumor site at 24 h post injection (Figure 2(a) to (d)). The F8IL9F8 variant with two scFv antibody moieties was found to be superior when compared to the two other variants (IL9F8 and F8IL9, respectively) in terms of biodistribution profile, with an increased accumulation at the tumor site and at least a 2-fold increase in the tumor to blood ratios (Figure 2(a)

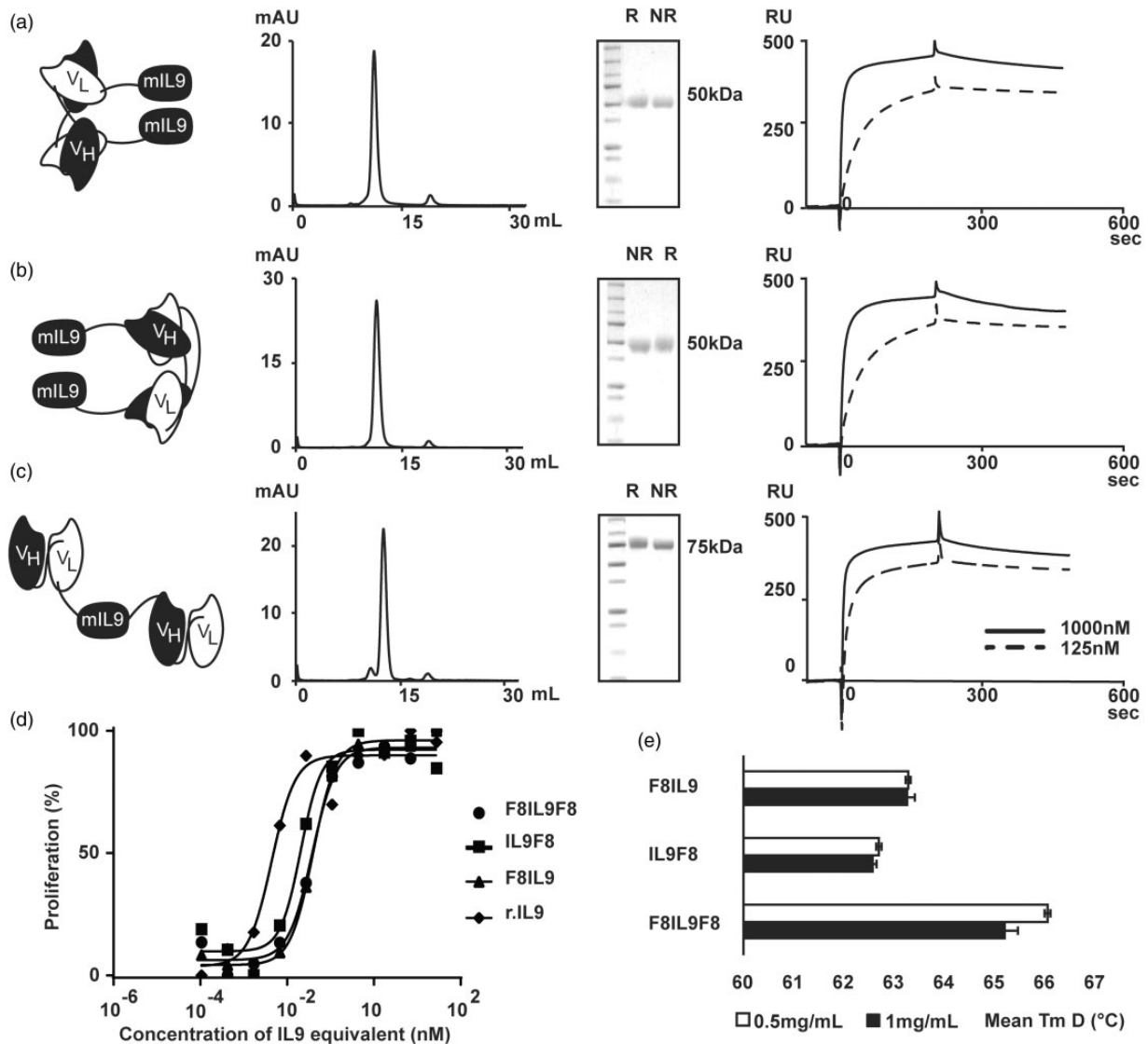


**Figure 1.** Cloning expression and characterization of IL9-based fusion proteins. IL9 fusion proteins have been expressed in CHO cells and characterized. From left to right: schematic representation of the IL9-based fusion protein, size exclusion chromatography profile, analytical SDS-PAGE analysis, SPR sensograms on EDA-coated sensor chip of (a) IL9F8, (b) F8IL9, (c) F8IL9F8. R: reducing conditions; NR: non-reducing conditions. (d) The proliferation of MC/9 has been assessed in presence of serial dilution of (■) IL9F8, (▲) F8IL9, (●) F8IL9F8, and (◆) commercially available recombinant murine IL9 produced in bacteria. Data are presented as percentage of maximal proliferation (mean of three replicates). (e) Thermal shift assay was performed on IL9-based fusion protein. Data are expressed in °C + Std. Error, melting temperature (T<sub>m</sub>) was assessed at two different protein concentrations.

and (b)). For further *in vivo* investigation, we decided to focus on F8IL9F8 due to its better targeting performance.

### IL9 fusion proteins display a therapeutic effect depending on cancer type tested

The therapeutic efficacy of F8IL9F8 was tested in three different cancer models: K1735M2 melanoma, CT26 colon carcinoma, and F9 teratocarcinoma.

Since previous studies showed the ability of IL9 or IL9-expressing Th9 cells to inhibit melanoma growth and reduce the number of melanoma-derived lung metastases in mouse,<sup>13,38</sup> F8IL9F8 was initially tested in the EDA-positive K1735M2 melanoma model.<sup>29</sup> Compared to the saline group, F8IL9F8 treatment exhibited minor tumor growth retardation which was statistically significant at the end point of the therapy (Figure 3(a)). Both F8IL9F8

and KSFIL9KSF treatments were well tolerated by mice, which displayed minimal and reversible weight loss. However, no substantial differences in tumor growth retardation and body weight change were observed between the treatments with targeted F8IL9F8 and the untargeted variant KSFIL9KSF (based on the irrelevant anti-hen egg lysozyme antibody KSF) (Figure 3(a)). The CT26 model, recently described as an immunologically “hot” tumor,<sup>39</sup> was investigated due to earlier reports demonstrating *in vivo* growth impairment of CT26 tumors ectopically expressing IL9<sup>14,15</sup> In order to investigate dose dependence effect of IL9 therapy, mice received three injections of F8IL9F8 at different doses, i.e. 100 μg or 200 μg. Both treatment regimens resulted in a similar tumor growth retardation when compared to the saline group, and no apparent signs of toxicity were reported (Figure 3(b)). However,

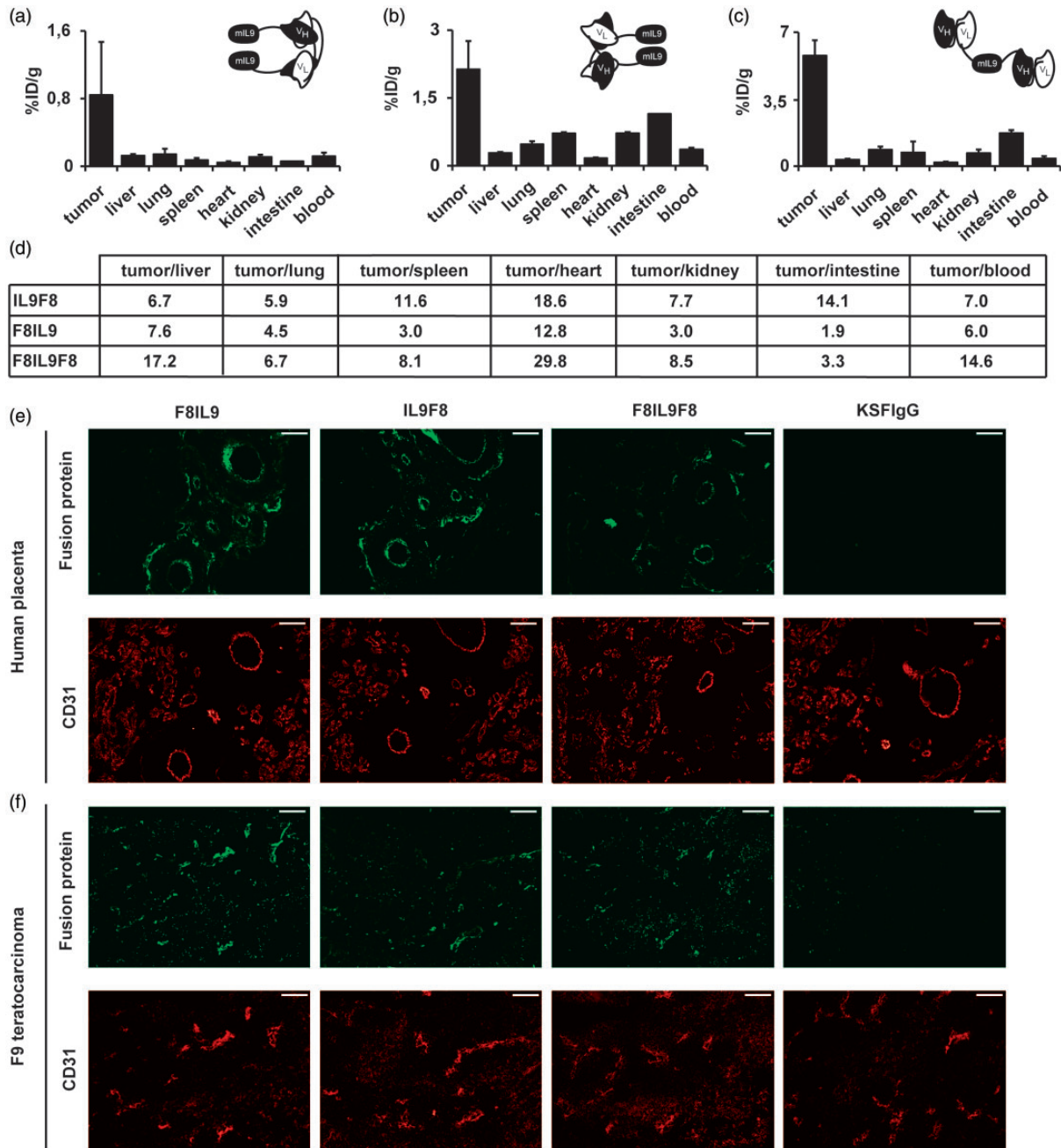


**Figure 2.** Tumor targeting performance of IL9-based immunocytokines. Quantitative biodistribution analysis of IL9-based fusion proteins; 10  $\mu$ g of (a) IL9F8, (b) F8IL9, and (c) F8IL9F8 radiolabeled protein have been injected into the lateral tail vein of F9 tumor bearing mice. Organs were collected, weighed, and the radioactivity measured 24 h after injection. Results are expressed as percentage of injected dose per gram of tissue (% ID/g  $\pm$  SEM), ( $n = 3$  mice). (d) Table of tumor to organ ratios calculated from the average of the % ID/g. (e and f) Microscopic fluorescence analysis of (top panels) biotinylated IL9-based fusions proteins and (lower panels) anti CD31 antibody. Staining has been done against (e) healthy human placenta and (f) F9 Tumors grown in 129 Sv mice, 10 $\times$  magnification and scale bar represent 50  $\mu$ m. The irrelevant KSF antibody in IgG format was used as negative control. (A color version of this figure is available in the online journal.)

similar to K1735M2 melanoma, also in the CT26 model no tumor eradication and mouse cure could be achieved with F8IL9F8. No therapeutic benefit of F9IL9F8 was observed in comparison to the saline group or mice treated with KSFIL9KSF in the F9 teratocarcinoma model. Interestingly, in this particular tumor model, treatment with F8IL9F8 and KSFIL9KSF resulted in the highest body weight loss (Figure 3(c)).

To confirm the *in vivo* targeting ability of F8IL9F8 in these therapies setting, *ex vivo* immunofluorescence studies were

performed. In parallel to the therapy studies, additional K1735M2, CT26, and F9 tumor bearing mice were injected with FITC-labeled fusion protein variants, sacrificed after 24h and tumors were analyzed for the localization of the injected fusion proteins within the tumor mass. A preferential accumulation of F8IL9F8 around the neovasculature structures was observed for the three tumor models tested, by contrast no signal was observed for KSFIL9KSF or PBS injected mice, confirming the efficient and selective tumor targeting of the F8IL9F8 protein (Figure 3(d)).

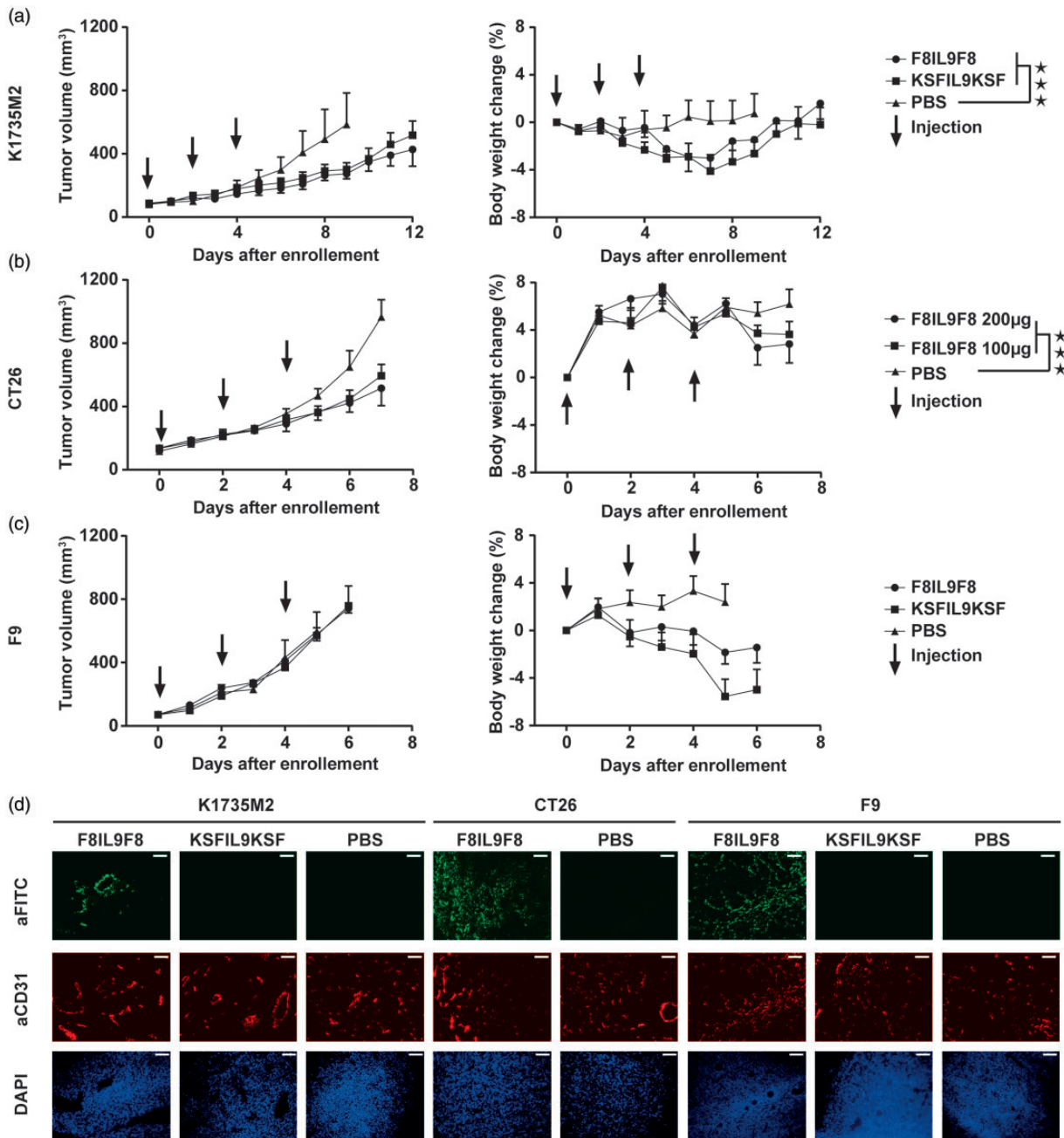


**Figure 3.** Therapeutic performance of IL9-based immunocytokines in C3H bearing K1735M2 melanoma, in Balb/c bearing CT26 colon carcinoma, and in Sv129 bearing F9 teratocarcinoma. Comparison of F8IL9F8, KSFIL9KSF injected at 200 µg, and PBS, treatment started when K1735M2 reached an average volume of 100 mm<sup>3</sup> borne in C3H ( $n = 5$  mice for F8IL9F8 and KSFIL9KSF and  $n = 4$  for PBS). (a) Comparison of F8IL9F8 injected at 200 µg, at 100 µg and PBS, treatment started when CT26 tumors reached a volume of 120 mm<sup>3</sup> borne in Balb/c mice ( $n = 5$  mice per group) (b) and comparison of F8IL9F8, KSFIL9KSF injected at 200 µg, and PBS, treatment started when F9 tumors reached an average volume of 72 mm<sup>3</sup> borne in Sv129 ( $n = 5$  mice per group). (c) For all therapy experiments, mice were injected three times every second day i.v. in the lateral tail vein. Data represent mean tumor volume  $\pm$  SEM (a–c left panel), and body weight change  $\pm$  SEM (a–c right panel). Statistical analysis was performed on tumor volumes using a two-way Anova with a Bonferroni post-test ★ $P$ -value  $< 0.05$ , ★★ $P$ -value  $< 0.01$ , ★★★ $P$ -value  $< 0.001$ , ns: not significant. Microscopic immunofluorescence analysis of the targeting ability of F8IL9F8, compared to KSFIL9KSF and PBS on the three tested cancer models, 10 $\times$  magnification and scale bar represent 50 µm (d). (A color version of this figure is available in the online journal.)

### IL9 treatment is modifying the immune phenotype of tumors

The two models responsive to IL9 therapy (i.e. K1735M2 and CT26) were analyzed for immune cells infiltrates at the end of therapeutic treatment. Multiple representative pictures for each treatment group were analyzed by ImageJ to quantify the percentage of positive area following staining for CD4+

T, CD8+ T, Treg, and NK cells. A general increase in immune cells could be detected in both K1735M2 and CT26 tumors treated with IL9-fusion at 200 µg per injection (Figure 4), however to a degree considerably lower when compared to our previous reports with other targeted immunocytokines and different tumor models.<sup>30,40–45</sup> Interestingly, in K1735M2 melanomas, a comparable increment in CD4+T and CD8+T cells was observed in mice treated with either

F8IL9F8 or KSFIL9KSF, whereas a slight increment in NK cells was observed only for F8IL9F8. Furthermore, no relevant changes in the infiltration of Treg cells could be observed between the three tested articles (Figure 4(a) and (c)). Similar results were obtained for the CT26 colon carcinoma model, with a moderate increase of infiltrated CD4, CD8, and NK cells (Figure 4(b) and (d)).

#### Delivery of IL-9 at the site of the disease did not provide a therapeutic benefit as an anti-inflammatory agent in collagen-induced arthritis mouse model

The therapeutic potential of F8IL9F8 for the treatment of rheumatoid arthritis (RA) has been assessed in the CIA murine model. The disease was induced by two injections of a Bovine collagen preparation at distinct time points,

which led to a rapid development of the disease. Mice were scored every other day using the standard scoring system. For each paw, mice received 1 score for one toe inflamed and swollen, 2 for more than one toe, but not entire paw inflamed and swollen or mild inflammation and swollen paw, 3 for the entire paw inflamed and swollen, and 4 for very inflamed and swollen paw. At the onset of the disease, F8IL9F8 was injected either at high (150  $\mu\text{g}/\text{dose}$ ) or low (50  $\mu\text{g}/\text{dose}$ ) dose, and dexamethasone or PBS treatments were used as positive and negative controls, respectively. Whereas the positive control dexamethasone effectively reduced the diseases score already after three days from beginning of the treatment, the disease progression in the animal treated either with 50 or 150  $\mu\text{g}/\text{dose}$  F8IL9F8 was comparable to the one of the mice in the

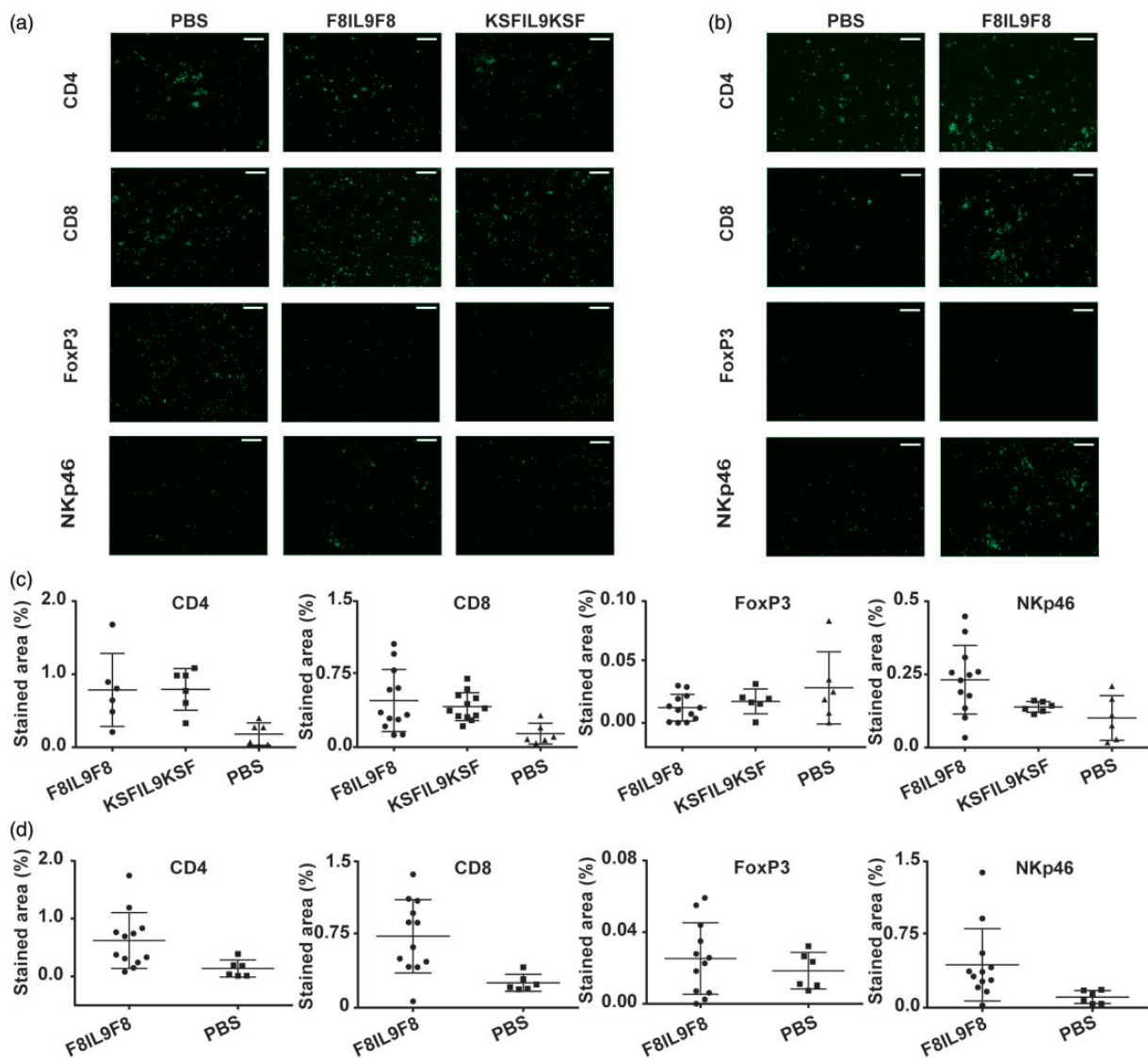


**Figure 4.** Immunofluorescence analysis on tumor-infiltrating immune cells in K1735M2 melanoma and CT26 colon carcinoma. Immunocompetent mice bearing K1735M2 (a and c) and CT26 (b and d) were injected three times every second day i.v. with 200  $\mu\text{g}$  F8IL9F8, or 200  $\mu\text{g}$  KSFIL9KSF or PBS. Mice were sacrificed 24 h after the last injection and tumor sections were stained for CD4<sup>+</sup> cells (CD4), CD8<sup>+</sup> cells (CD8), Tregs (FoxP3), and NK cells (NKp46) ( $n = 2$  mice for F8IL9F8  $n = 1$  for KSFIL9KSF and PBS). Microscopic analysis of a representative section for each immunofluorescence, 10 $\times$  magnification and scale bar represent 50  $\mu\text{m}$  (a and b). Quantification of percentage of stained area using Image J. For each stained sections, six representative areas were quantified and plotted as single dots, bars correspond to mean values with standard deviation (c and d). Full set of pictures used for quantification of area are represented in Figure S1. (A color version of this figure is available in the online journal.)

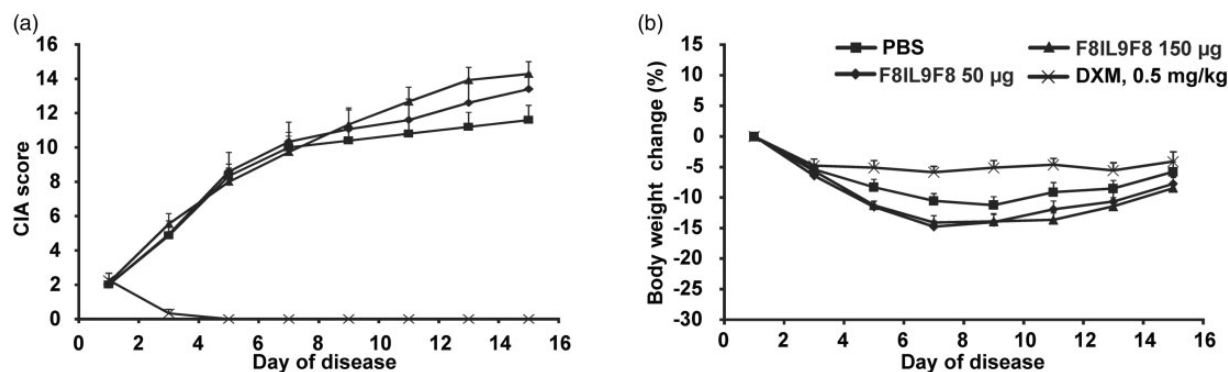


**Figure 5.** Therapeutic performance of F8IL9F8 in collagen-induced arthritis (CIA) DBA/1 mice. Comparison of F8IL9F8, vehicle (PBS), and dexamethasone treatment in collagen-induced arthritis DBA/1 mice. At the onset of the disease (day 1), arthritic mice were injected three times every second day i.v. in the lateral tail vein with F8IL9F8 (150 µg or 50 µg) or vehicle (PBS). Dexamethasone was daily administrated (0.5 mg/kg) i.p. from the onset of the disease. ( $n = 15$  mice per group). Data represent from the onset of the disease mean CIA score  $\pm$  SEM (a), body weight change from day 1 in percentage  $\pm$  SEM (b).

saline group (Figure 5(a)). In agreement with the arthritic score increase, mice treated with F8IL9F8 or PBS showed a more prominent, yet reversible, body weight loss when compared to the positive control group treated with dexamethasone (Figure 5(b)).

## Discussion

We have generated and characterized three novel formats for antibody fusions with murine IL9. All three immunocytokine variants based on the F8 antibody, specific to the alternatively spliced EDA domain of fibronectin, could be expressed and purified to homogeneity. The products retained antigen-binding properties as well as *in vitro* IL9 biological activity. In our *in vitro* assay, the three immunocytokine showed an about 5 to 10-fold reduced bioactivity compared to a commercial IL9 preparation used as control. Differences in the methods used for sample quantification may contribute to such dissimilarity. In fact, while the three recombinant immunocytokines were quantified by spectrophotometric measurement, for the concentration of the commercial IL9 sample we relied on the information provided by the supplier. In alternative, it may be speculated that the fusion of IL9 to the antibody moieties may decrease its affinity to the IL9 receptor. In the latter case, we expect that the antibody mediated accumulation of IL9 at the disease site will compensate for its potential reduction in bioactivity; furthermore, an attenuated IL9 activity could be beneficial for *in vivo* applications, as it would reduce systemic toxicity of the immunocytokine during diffusion through the body. Immunocytokines based on attenuated cytokines variants are increasingly being explored as a strategy to reduce systemic toxicity.<sup>46,47</sup> However, additional *in vitro* activity and receptor binding experiments using alternative IL9 preparations will be required to confirm the potential reduction in bioactivity of the three fusion proteins.

The F8IL9F8 product exhibited the best tumor targeting performance (6% ID/g in the tumor at 24h), with a tumor:blood ratio of 14.6. The percent injected dose per gram of tissue of IL9-fusions that could be delivered to tumors in mice was comparable to results obtained for other F8-fusion proteins with other cytokine payloads (e.g., IL2, IL4,

IL6, IL10, IL12, TNF, interferon-alpha).<sup>27,30,48–52</sup> However, unlike other F8-based immunocytokines,<sup>27,30,48–52</sup> F8IL9F8 did not display a potent anti-cancer activity *in vivo*. Similarly, F8IL9F8 was not active in a mouse model of arthritis.

The function of IL9 in tumor immunity is controversial.<sup>53–55</sup> It has been generally suggested that IL9 may inhibit the growth of solid tumors by activating the innate or adaptive immune response,<sup>56,57</sup> while as a lymphocyte growth factor it may promote progression of hematological malignancies.<sup>10,12</sup> However, since IL9 has also been reported to promote proliferation of multiple solid tumor models (like pancreatic cancer, lung cancer, and colitis associated cancer),<sup>58–60</sup> its anti-cancer activity may be context and tumor type specific.<sup>53–55</sup>

In this study, we have used three syngeneic immunocompetent models of solid cancer known to express the EDA antigen (i.e. K1735M2 melanoma, CT26 colon carcinoma, and F9 teratocarcinoma, respectively). When compared to saline treatment, a moderate anti-tumor effect could be observed *in vivo* only in the K1735M2 and CT26 models. However, targeting of F8IL9F8 did not result in improved therapeutic efficacy compared to the untargeted KSFIL9KSF at corresponding doses.

The antitumor function of IL9 on melanoma was initially postulated by Purwar and collaborators who showed that adoptive transfer of IL9-producing Th9 cells in mice bearing B16F10 melanoma tumors was highly efficient in preventing tumor progression.<sup>13</sup> Accordingly, injection of recombinant IL9 resulted in impaired tumor growth, although to a lesser extent. More recently, Park and collaborators used B16F10 melanoma cells ectopically expressing soluble or membrane bound forms of IL9 to demonstrate the ability of IL9 to inhibit lung metastases.<sup>61</sup> A similar approach was used by Do Thi and collaborators. In this case, CT26 colon cancer cells engineered to ectopically express a membrane bound IL9, showed tumor growth retardation when compared to mock transfected CT26 cells.<sup>14,15</sup> The exact mechanisms underlying IL9-mediated anti-tumor immunity are not fully understood. Whereas a prominent increase of CD4+ and CD8+ T and NK cells have been reported in tumor models ectopically expressing

IL9,<sup>14,61</sup> the work of Purwar suggest a key role played by mast cells since IL9-mediated tumor growth inhibition was abrogated in Kit W-sh mice (mast cells deficient mice).<sup>13</sup> With our approach, we expected that high IL9 concentrations at tumor site, resulting from the antibody-mediated targeted delivery of IL9, could contribute to a strong pro-inflammatory environment ideally favoring anti-cancer immunity and tumor eradication. Even though *in vivo* targeting of IL9 to the subendothelial matrix of the tested tumor models was successful, only moderate tumor growth retardation could be obtained. Similarly, only a very modest increase in tumor infiltrating CD4+ T, CD8+ T and NK cells could be observed in the two IL9 responsive models (i.e. K1735M2 and CT26). Similar findings have been reported by our groups: other F8 delivered payloads (e.g. IL17, IFN $\alpha$ , and calreticulin) could increase immune cells infiltration without leading to noticeable anti-cancer efficacy in immunocompetent mice.<sup>62–64</sup> By contrast, other immunocytokines (e.g. IL2, IL12, IL15, TNF) can promote strong neoplastic mass immune cells infiltration and strong anti-tumor efficacy.<sup>40,44,45,48,65,66</sup>

In a more recent study, Rauber and collaborators showed that IL9 could resolve chronic inflammation in two different models of arthritis (i.e. AIA in IL9 deficient mice and SIA models).<sup>16</sup> They identified IL9-producing ILC2 cells as main mediators of the resolution of the chronic inflammation and proposed a mechanism by which IL9 would support ILC2 proliferation and survival by an autocrine loop. In our study, we did not observe a therapeutic benefit when F8IL9F8 was administered to arthritic mice. Both differences in the murine arthritis models and therapeutic approach used may account for the divergent results. The CIA model was chosen since in this model we previously demonstrate strong EDA expression in the arthritic paws that were efficiently targeted by various F8-based immunocytokines.<sup>27,31,33</sup> Recombinant F8IL9F8 was administered after the onset of the disease in order to mimic as close as possible a potential clinical setting. By contrast, the studies of Rauber are based on non-standard therapy experiments that would be difficult to be directly translated into clinical practice. IL9 was delivered by hydrodynamic gene transfer (HDGT) approach which do not allow control over the timing and concentration of overexpressed IL9. Furthermore, in their AIA study, IL9 deficient mice were used, in which a chronic form of arthritis is developed, without signs of resolution. It should be noticed that whereas restoration of IL9 expression in the knockout mice could resolve chronic inflammation, no therapeutic benefit was observed in the wild type mice. Finally, in their serum-induced arthritis model (SIA), IL9 delivery by HDGT was performed five days before disease induction, this would mimic a prophylactic rather than a therapeutic approach. The potential therapeutic benefit mediated by IL9 prior to the onset of the disease is in line with the recent finding that in the same SIA model, ILC2 adoptive transfer attenuated arthritis only if performed before SIA induction.<sup>67</sup>

The therapeutic results obtained in the preclinical models of cancer and arthritis with F8IL9F8 were unexpected, particularly considering the previous results published by Purwar and Rauber.<sup>13,16</sup> Although, it remains to be

tested whether the anti-cancer and anti-arthritis activity of F8IL9F8 can be improved by combining it with other immunocytokines or through a prophylactic approach, respectively, currently, we do not believe that IL9 represents a suitable payload for the development of anti-tumor or anti-arthritis immunocytokines.

#### AUTHORS' CONTRIBUTIONS

BG, MM, and DN designed research. BG, carried out the experiment. TO, SC, RDL. AK contributed to the *in vivo* experiments and sample preparation. BG, MM, and DN wrote the paper with input from all the authors. PV contributed to the implementation of the research, and to the writing of the manuscript.

#### ACKNOWLEDGMENTS

We thank Catherine Pemberton-Ross and Lottie Howell for help with protein engineering and production.

#### DECLARATION OF CONFLICTING INTERESTS

DN is a co-founder and shareholder of Philogen SpA, the company that owns the F8 antibody. BG, TO, SC, RDL, AK, AV, and MM are employees of Philochem AG, daughter company of Philogen acting as discovery unit of the group. PV has no conflict of interest to declare. A patent is pending on the format and use of F8-IL9 Immunocytokines.

#### FUNDING

Financial support by the ETH Zürich, the Swiss National Science Foundation (grant number 310030\_182003/1), the European Research Council (ERC) under the European Union's Horizon 2020 research and innovation program (grant agreement 670603) is gratefully acknowledged.

#### ORCID iD

Mattia Matasci  <https://orcid.org/0000-0003-4221-8852>

#### SUPPLEMENTAL MATERIAL

Supplemental material for this article is available online.

#### REFERENCES

- Goswami R, Kaplan MH. A brief history of IL-9. *J Immunol* 2011;**186**:3283–8
- Noelle RJ, Nowak EC. Cellular sources and immune functions of interleukin-9. *Nat Rev Immunol* 2010;**10**:683–7
- Schmitt E, Germann T, Goedert S, Hoehn P, Huels C, Koelsch S, Kühn R, Müller W, Palm N, Rüde E. IL-9 production of naive CD4+ T cells depends on IL-2, is synergistically enhanced by a combination of TGF-beta and IL-4, and is inhibited by IFN-gamma. *J Immunol* 1994;**153**:3989–96
- Renauld JC, Druet C, Kermouni A, Houssiau F, Uyttenhove C, Van Roost E, Van Snick J. Expression cloning of the murine and human interleukin 9 receptor cDNAs. *Proc Natl Acad Sci USA* 1992;**89**:5690–4
- Licona-Limón P, Henao-Mejia J, Temann AU, Gagliani N, Licona-Limón I, Ishigame H, Hao L, Herbert DR, Flavell RA. Th9 cells drive host immunity against gastrointestinal worm infection. *Immunity* 2013;**39**:744–57
- Turner J-E, Morrison PJ, Wilhelm C, Wilson M, Ahlfors H, Renauld J-C, Panzer U, Helmby H, Stockinger B. IL-9-mediated survival of type 2

- innate lymphoid cells promotes damage control in helminth-induced lung inflammation. *J Exp Med* 2013;**210**:2951–65
7. Koch S, Soppel N, Finotto S. Th9 and other IL-9-producing cells in allergic asthma. *Semin Immunopathol* 2017;**39**:55–68
  8. Hauber H-P, Bergeron C, Hamid Q. IL-9 in allergic inflammation. *Int Arch Allergy Immunol* 2004;**134**:79–87
  9. Vargas Humblin RT, Végran E, Ghiringhelli F, Apetoh F. L. TH9 cells in anti-tumor immunity. *Semin Immunopathol* 2017;**39**:39–46
  10. Chen N, Lu K, Li P, Lv X, Wang X. Overexpression of IL-9 induced by STAT6 activation promotes the pathogenesis of chronic lymphocytic leukemia. *Int J Clin Exp Pathol* 2014;**7**:2319–23
  11. Renaud JC, van der Lugt N, Vink A, van Roon M, Godfraind C, Warnier G, Merz H, Feller A, Berns A, Van Snick J. Thymic lymphomas in interleukin 9 transgenic mice. *Oncogene* 1994;**9**:1327–32
  12. Zhang J, Wang W, Geng Q-R, Wang L, Chen X-Q, Liu C-C, Lv Y. Serum levels of interleukin-9 correlate with negative prognostic factors in extranodal NK/T-cell lymphoma. *PLoS One* 2014;**9**:e94637
  13. Purwar R, Schlaapbach C, Xiao S, Kang HS, Elyaman W, Jiang X, Jetten AM, Khoury SJ, Fuhlbrigge RC, Kuchroo VK, Clark RA, Kupper TS. Robust tumor immunity to melanoma mediated by interleukin-9-producing T cells. *Nat Med* 2012;**18**:1248–53
  14. D, Thi VA, Park SM, Lee H, Kim YS. Ectopically expressed membrane-bound form of IL-9 exerts immune-stimulatory effect on CT26 Colon carcinoma cells. *Immune Netw* 2018;**18**:e12
  15. Wang J, Sun M, Zhao H, Huang Y, Li D, Mao D, Zhang Z, Zhu X, Dong X, Zhao X. IL-9 exerts antitumor effects in colon cancer and transforms the tumor microenvironment in vivo. *Technol Cancer Res Treat* 2019;**18**:1533033819857737.
  16. Rauber S, Lubert M, Weber S, Maul L, Soare A, Wohlfahrt T, Lin N-Y, Dietel K, Bozec A, Herrmann M, Kaplan MH, Weigmann B, Zaiss MM, Fearon U, Veale DJ, Cañete JD, Distler O, Rivellese F, Pitzalis C, Neurath MF, McKenzie ANJ, Wirtz S, Schett G, Distler JHW. Ramming A. Resolution of inflammation by interleukin-9-producing type 2 innate lymphoid cells. *Nat Med* 2017;**23**:938–44
  17. Neri D, Sondel PM. Immunocytokines for cancer treatment: past, present and future. *Curr Opin Immunol* 2016;**40**:96–102
  18. Bootz F, Neri D. Immunocytokines: a novel class of products for the treatment of chronic inflammation and autoimmune conditions. *Drug Discov Today* 2016;**21**:180–9
  19. Pasche N, Neri D. Immunocytokines: a novel class of potent armed antibodies. *Drug Discov Today* 2012;**17**:583–90
  20. Venetz D, Hess C, Lin C, Aebi M, Neri D. Glycosylation profiles determine extravasation and disease-targeting properties of armed antibodies. *Proc Natl Acad Sci USA* 2015;**112**:2000–5
  21. Villa A, Trachsel E, Kaspar M, Schliemann C, Sommariva R, Rybak J-N, Rösl C, Borsi L, Neri D. A high-affinity human monoclonal antibody specific to the alternatively spliced EDA domain of fibronectin efficiently targets tumor neo-vasculature in vivo. *Int J Cancer* 2008;**122**:2405–13
  22. Rybak J-N, Trachsel E, Scheuermann J, Neri D. Ligand-based vascular targeting of disease. *Chem Med Chem* 2007;**2**:22–40
  23. Schwager K, Villa A, Rösli C, Neri D, Rösli-Khabas M, Moser G. A comparative immunofluorescence analysis of three clinical-stage antibodies in head and neck cancer. *Head Neck Oncol* 2011;**3**:25
  24. Schliemann C, Palumbo A, Zuberbühler K, Villa A, Kaspar M, Trachsel E, Klapper W, Messens HD, Neri D. Complete eradication of human B-cell lymphoma xenografts using rituximab in combination with the immunocytokine L19-IL2. *Blood* 2009;**113**:2275–83
  25. Gutbrodt KL, Schliemann C, Giovannoni L, Frey K, Pabst T, Klapper W, Berdel WE, Neri D. Antibody-based delivery of interleukin-2 to neovasculature has potent activity against acute myeloid leukemia. *Sci Transl Med* 2013;**5**:201ra118
  26. Schwager K, Bootz F, Imesch P, Kaspar M, Trachsel E, Neri D. The antibody-mediated targeted delivery of interleukin-10 inhibits endometriosis in a syngeneic mouse model. *Hum Reprod* 2011;**26**:2344–52
  27. Schwager K, Kaspar M, Bootz F, Marcolongo R, Paresce E, Neri D, Trachsel E. Preclinical characterization of DEKAVIL (F8-IL10), a novel clinical-stage immunocytokine which inhibits the progression of collagen-induced arthritis. *Arthritis Res Ther* 2009;**11**:R142
  28. Bootz F, Venetz D, Ziffels B, Neri D. Different tissue distribution properties for glycosylation variants of fusion proteins containing the p40 subunit of murine interleukin-12. *Protein Eng Des Sel* 2016;**29**:445–55
  29. Pretto F, Elia G, Castioni N, Neri D. Preclinical evaluation of IL2-based immunocytokines supports their use in combination with dacarbazine, paclitaxel and TNF-based immunotherapy. *Cancer Immunol Immunother* 2014;**63**:901–10
  30. Pasche N, Wulhfard S, Pretto F, Carugati E, Neri D. The antibody-based delivery of interleukin-12 to the tumor neovasculature eradicates murine models of cancer in combination with paclitaxel. *Clin Cancer Res* 2012;**18**:4092–103
  31. Hemmerle T, Doll F, Neri D. Antibody-based delivery of IL4 to the neovasculature cures mice with arthritis. *Proc Natl Acad Sci USA* 2014;**111**:12008–12
  32. Hemmerle T, Zgraggen S, Matasci M, Halin C, Detmar M, Neri D. Antibody-mediated delivery of interleukin 4 to the neo-vasculature reduces chronic skin inflammation. *J Dermatol Sci* 2014;**76**:96–103
  33. Doll F, Schwager K, Hemmerle T, Neri D. Murine analogues of etanercept and of F8-IL10 inhibit the progression of collagen-induced arthritis in the mouse. *Arthritis Res Ther* 2013;**15**:R138
  34. Bootz F, Ziffels B, Neri D. Antibody-based targeted delivery of interleukin-22 promotes rapid clinical recovery in mice with DSS-Induced colitis. *Inflamm Bowel Dis* 2016;**22**:2098–105
  35. Bruijnen STG, Chandrupatla DMSH, Giovanoni L, Neri D, Vugts DJ, Huisman MC, Hoekstra OS, Musters RJP, Lammertsma AA, van Dongen GAMS, Jansen G, Molthoff CFM, van der Laken CJ. F8-IL10: a new potential antirheumatic drug evaluated by a PET-Guided translational approach. *Mol Pharm* 2019;**16**:273–81
  36. Hacker DL, Kiseljak D, Rajendra Y, Thurnheer S, Baldi L, Wurm FM. Polyethyleneimine-based transient gene expression processes for suspension-adapted HEK-293E and CHO-DG44 cells. *Protein Exp Purif* 2013;**92**:67–76
  37. Pfaffen S, Frey K, Stutz I, Roesli C, Neri D. Tumour-targeting properties of antibodies specific to MMP-1A, MMP-2 and MMP-3. *Eur J Nucl Med Mol Imaging* 2010;**37**:1559–65
  38. Lu Y, Hong S, Li H, Park J, Hong B, Wang L, Zheng Y, Liu Z, Xu J, He J, Yang J, Qian J, Yi Q. Th9 cells promote antitumor immune responses in vivo. *J Clin Invest* 2012;**122**:4160–71
  39. Mosely SIS, Prime JE, Sainson RCA, Koopmann J-O, Wang DYQ, Greenawalt DM, Ahdesmaki MJ, Leyland R, Mullins S, Pacelli L, Marcus D, Anderton J, Watkins A, Coates Ulrichsen J, Brohawn P, Higgs BW, McCourt M, Jones H, Harper JA, Morrow M, Valge-Archer V, Stewart R, Dovedi SJ, Wilkinson RW. Rational selection of syngeneic preclinical tumor models for immunotherapeutic drug discovery. *Cancer Immunol Res* 2017;**5**:29–41
  40. Carnemolla B, Borsi L, Balza E, Castellani P, Meazza R, Berndt A, Ferrini S, Kosmehl H, Neri D, Zardi L. Enhancement of the antitumor properties of interleukin-2 by its targeted delivery to the tumor blood vessel extracellular matrix. *Blood* 2002;**99**:1659–65
  41. Halin C, Rondini S, Nilsson F, Berndt A, Kosmehl H, Zardi L, Neri D. Enhancement of the antitumor activity of interleukin-12 by targeted delivery to neovasculature. *Nat Biotechnol* 2002;**20**:264–9
  42. Ebbinghaus C, Ronca R, Kaspar M, Grabulovski D, Berndt A, Kosmehl H, Zardi L, Neri D. Engineered vascular-targeting antibody-interferon-gamma fusion protein for cancer therapy. *Int J Cancer* 2005;**116**:304–13
  43. Pedretti M, Rancic Z, Soltermann A, Herzog BA, Schliemann C, Lachat M, Neri D, Kaufmann PA. Comparative immunohistochemical staining of atherosclerotic plaques using F16, F8 and L19: three clinical-grade fully human antibodies. *Atherosclerosis* 2010;**208**:382–9
  44. Puca E, Probst P, Stringhini M, Murer P, Pellegrini G, Cazzamalli S, Huttmacher C, Gouyou B, Wulhfard S, Matasci M, Villa A, Neri D. The antibody-based delivery of interleukin-12 to solid tumors boosts NK and CD8+ T cell activity and synergizes with immune checkpoint inhibitors. *Int J Cancer* 2020;**146**:2518–30
  45. Schwager K, Hemmerle T, Aebischer D, Neri D. The immunocytokine L19-IL2 eradicates cancer when used in combination with CTLA-4 blockade or with L19-TNF. *J Invest Dermatol* 2013;**133**:751–8
  46. Pogue SL, Taura T, Bi M, Yun Y, Sho A, Mikesell G, Behrens C, Sokolovsky M, Hallak H, Rosenstock M, Sanchez E, Chen H,

- Berenson J, Doyle A, Nock S, Wilson DS. Targeting attenuated interferon- $\alpha$  to myeloma cells with a CD38 antibody induces potent tumor regression with reduced off-Target activity. *PLoS One* 2016;**11**:e0162472
47. Cauwels A, Van Lint S, Garcin G, Bultinck J, Paul F, Gerlo S, Van der Heyden J, Bordat Y, Catteuw D, De Cauwer L, Rogge E, Verhee A, Uzé G, Tavernier J. A safe and highly efficient tumor-targeted type I interferon immunotherapy depends on the tumor microenvironment. *Oncoimmunology* 2017;**7**:e1398876
48. Hess C, Neri D. The antibody-mediated targeted delivery of interleukin-13 to syngeneic murine tumors mediates a potent anticancer activity. *Cancer Immunol Immunother* 2015;**64**:635–44
49. Hess C, Neri D. Tumor-targeting properties of novel immunocytokines based on murine IL1 $\beta$  and IL6. *Protein Eng Des Sel* 2014;**27**:207–13
50. Hemmerle T, Neri D. The dose-dependent tumor targeting of antibody-IFN $\gamma$  fusion proteins reveals an unexpected receptor-trapping mechanism in vivo. *Cancer Immunol Res* 2014;**2**:559–67
51. Hutmacher C, Núñez NG, Liuzzi AR, Becher B, Neri D. Targeted delivery of IL2 to the tumor stroma potentiates the action of immune checkpoint inhibitors by preferential activation of NK and CD8 $^+$  T cells. *Cancer Immunol Res* 2019;**7**:572–83
52. Hemmerle T, Probst P, Giovannoni L, Green AJ, Meyer T, Neri D. The antibody-based targeted delivery of TNF in combination with doxorubicin eradicates sarcomas in mice and confers protective immunity. *Br J Cancer* 2013;**109**:1206–13
53. Wan J, Wu Y, Ji X, Huang L, Cai W, Su Z, Wang S, Xu H. IL-9 and IL-9-producing cells in tumor immunity. *Cell Commun Signal* 2020;**18**:50
54. Chen T, Guo J, Cai Z, Li B, Sun L, Shen Y, Wang S, Wang Z, Wang Z, Wang Y, Zhou H, Cai Z, Ye Z. Th9 cell differentiation and its dual effects in tumor development. *Front Immunol* 2020;**11**:1026.
55. Lee JE, Zhu Z, Bai Q, Brady TJ, Xiao H, Wakefield MR, Fang Y. The role of interleukin-9 in cancer. *Pathol Oncol Res* 2020;**26**:2017–22
56. Schmitt E, Klein M, Bopp T. Th9 cells, new players in adaptive immunity. *Trends Immunol* 2014;**35**:61–8
57. Ramadan A, Griesenauer B, Adom D, Kapur R, Hanenberg H, Liu C, Kaplan MH, Paczesny S. Specifically differentiated T cell subset promotes tumor immunity over fatal immunity. *J Exp Med* 2017;**214**:3577–96
58. Hu B, Qiu-Lan H, Lei R-E, Shi C, Jiang H-X, Qin S-Y. Interleukin-9 promotes pancreatic cancer cells proliferation and migration via the miR-200a/beta-catenin axis. *Biomed Res Int* 2017;**2017**:2831056
59. Tian L, Li Y, Chang R, Zhang P, Zhang J, Huo L. Lentiviral vector-mediated IL-9 overexpression stimulates cell proliferation by targeting c-myc and cyclin D1 in colitis-associated cancer. *Oncol Lett* 2019;**17**:175–82
60. Ye Z-J, Zhou Q, Yin W, Yuan M-L, Yang W-B, Xiong X-Z, Zhang J-C, Shi H-Z. Differentiation and immune regulation of IL-9-producing CD4 $^+$  T cells in malignant pleural effusion. *Am J Respir Crit Care Med* 2012;**186**:1168–79
61. Park SM, Do-Thi VA, Lee J-O, Lee H, Kim YS. Interleukin-9 inhibits lung metastasis of melanoma through stimulating anti-tumor M1 macrophages. *Mol Cells* 2020;**43**:479–90
62. Frey K, Zivanovic A, Schwager K, Neri D. Antibody-based targeting of interferon-alpha to the tumor neovasculature: a critical evaluation. *Integr Biol* 2011;**3**:468–78
63. Ziffels B, Grötsch A, Al-Bayati L, Neri D. Targeted delivery of calreticulin to ED-a fibronectin leads to tumor-growth retardation. *J Biotechnol* 2019;**290**:53–8
64. Pasche N, Frey K, Neri D. The targeted delivery of IL17 to the mouse tumor neo-vasculature enhances angiogenesis but does not reduce tumor growth rate. *Angiogenesis* 2012;**15**:165–9
65. De Luca R, Gouyou B, Ongaro T, Villa A, Ziffels B, Sannino A, Buttinoni G, Galeazzi S, Mazzacuva M, Neri D. A novel fully-human potency-matched dual cytokine-antibody fusion protein targets carbonic anhydrase IX in renal cell carcinomas. *Front Oncol* 2019;**9**:1228
66. Halin C, Gafner V, Villani ME, Borsi L, Berndt A, Kosmehl H, Zardi L, Neri D. Synergistic therapeutic effects of a tumor targeting antibody fragment, fused to interleukin 12 and to tumor necrosis factor  $\alpha$ . *Cancer Res* 2003;**63**:3202–10
67. Omata Y, Frech M, Primbs T, Lucas S, Andreev D, Scholtyssek C, Sarter K, Kindermann M, Yerenenko N, Baeten DL, Andreas N, Kamradt T, Bozec A, Ramming A, Krönke G, Wirtz S, Schett G, Zaiss MM. Group 2 innate lymphoid cells attenuate inflammatory arthritis and protect from bone destruction in mice. *Cell Rep* 2018;**24**:169–80

(Received September 16, 2020, Accepted November 24, 2020)